Force transmission through the inner kinetochore is enhanced by centromeric DNA sequences

Elise Miedlar[1*], Grace E. Hamilton[1**], Samuel R. Witus[1***], Sara Gonske[1], Michael Riffle[1****], Alex Zelter[1****], Rachel E. Klevit[1], Charles L. Asbury[2], Yoana N. Dimitrova[3], and Trisha N. Davis[1]

[1]Department of Biochemistry, University of Washington, Seattle, United States

[2]Department of Physiology and Biophysics, University of Washington, Seattle, United States

[3]Department of Structural Biology, Genentech, Inc., South San Francisco, United States

* Current address: University of Pennsylvania, Philadelphia, Pennsylvania, United States

** Current address: Department of Biochemistry, High Point University, High Point, North Carolina, United States

*** Current address: Department of Molecular and Cell Biology, University of California, Berkeley, United States

**** Current address: Department of Genome Sciences, University of Washington, Seattle United States

Abstract

Previously, we reconstituted a minimal functional kinetochore from recombinant *S. cerevisiae* proteins that was capable of transmitting force from dynamic microtubules to nucleosomes containing the centromere-specific histone variant Cse4 (Hamilton et al. 2020). This work revealed two paths of force transmission through the inner kinetochore: through Mif2 and through the Okp1/Ame1 complex (OA). Here, using a chimeric DNA sequence that contains crucial centromere-determining elements of the budding yeast point centromere, we demonstrate that the presence of centromeric DNA sequences in Cse4-containing nucleosomes significantly strengthens OA-mediated linkages. Our findings indicate that centromeric sequences are important for the transmission of microtubule-based forces to the chromosome.

Introduction

The kinetochore is an assembly of protein subcomplexes that links dynamic microtubule plus ends to chromosomes via centromeric nucleosomes (Ariyoshi and Fukagawa, 2023). Through this linkage, kinetochores transmit force from microtubules to chromosomes to align them on the metaphase plate during mitosis, putting both kinetochores and centromeres under tension. This tension signals that kinetochores are correctly bioriented and is a key aspect of the kinetochore's ability to regulate entry into mitosis and prevent aneuploidy (Akiyoshi et al., 2010; Nicklas and Ward, 1994).

Centromeres in most eukaryotes are defined by the presence of a centromere-specific histone variant, called Cse4 in budding yeast (also known as CENP-A). The yeast

“point” centromere is also defined by DNA sequence – approximately 125 bp in three centromere-determining elements, CDEI, CDEII and CDEIII (Clarke and Carbon, 1980; Clarke and Carbon, 1985). Both the Cse4-containing histone octamer and the centromere specific DNA elements provide a scaffold for kinetochore assembly. Previously, we showed that kinetochore assemblies built from recombinant *S. cerevisiae* proteins can transmit force through either Mif2 or OA as the inner kinetochore subcomplex binding the centromeric nucleosome (Hamilton et al., 2020). In that study, we used recombinant nucleosome core particles wrapped with the Widom 601 DNA (W601-NCPs), which has a sequence that wraps canonical histone octamers with high efficiency (Lowary and Widom, 1998). The Widom 601 sequence has also fortuitously enabled stable wrapping of centromeric histone octamers *in vitro* where it would not otherwise be possible. However, Widom 601 DNA does not contain any native centromeric DNA, and therefore we could not address the relationship between centromere-specific DNA and force transmission.

Here, we develop a chimeric DNA sequence (CCEN) that contains both native centromeric DNA and Widom 601 DNA to reconstitute centromeric nucleosomes. The chimera includes a portion of CDEII and all of CDEIII from the native centromere to allow for DNA-dependent binding between the nucleosome core particles (NCPs) and the kinetochore, as well as segments of Widom 601 DNA at the ends to facilitate stable wrapping. Centromeric histone octamers wrapped with CCEN DNA are stable and thus provide an opportunity to measure the contribution of DNA sequence to the strength of kinetochore attachments.

We found that OA-based assemblies withstood significantly higher forces when nucleosomes were wrapped in the centromere chimeric DNA, while we did not detect significant strengthening of Mif2-based assemblies based on the DNA sequence used to wrap nucleosomes. Our findings show that centromeric specific DNA sequence elements make significant contributions, either directly or indirectly, to the attachment strength between the inner kinetochore and the centromeric nucleosome.

Results

We produced nucleosome core particles (NCPs) by wrapping 147-bp long chimeric centromeric DNA (CCEN) or Widom 601 DNA (W601) around recombinant Cse4, H2A, H2B, and H4 histone octamers (Figure 1A). The latter three histones had a polyhistidine tag (His6) to facilitate purification and allow NCP binding to the polystyrene beads used in the optical trap rupture force assay. After the initial wrapping, NCPs were purified over a size exclusion chromatography column (Figure 1B and 1C). As in our previous study (Hamilton et al., 2020), we also purified five recombinant kinetochore subcomplexes that can self-assemble onto the NCPs to create a minimal, functional kinetochore: OA, Mif2, MIND, Ndc80c, and Dam1c.

Before determining the quantitative rupture strength that each kinetochore assembly could withstand, we confirmed that the recombinant elements could spontaneously build a functional kinetochore as previously described (Hamilton et al., 2020). Briefly, the NCPs bearing His6-tags were bound directly to polystyrene microbeads via anti-His6 antibodies. The remaining subcomplexes, which did not have His6-tags, were

added free in solution and bound to the beads only indirectly, by assembling together with the directly tethered, His6-tagged NCP. Using a laser trap to manipulate individual beads, we tested the kinetochore assemblies for their ability to bind microtubules. Each bead was brought to the dynamic plus end of a microtubule anchored onto the surface of the flow chamber. If the bead bound to the microtubule when released from the laser trap, then the kinetochore assembly was designated as functional, and the bead was used for the rupture force assay.

With either OA or Mif2 in solution, over 78% of beads coated in W601-NCPs or CCEN-NCPs could bind microtubules (Figure 2A, Table 1). Negative controls where OA or Mif2 was omitted from solution were also performed to confirm the specificity of the NCP for its inner kinetochore binding partner over the outer kinetochore components of the assembly. The negative controls showed 0% bead binding to microtubules, confirming that functional kinetochores are only assembled on NCPs when either OA or Mif2 is present in solution. After a bead was designated as functional, the rupture force of the assembled chain was tested as described in Materials and Methods.

W601 OA vs. CCEN OA

Although OA has not previously been reported to bind specific centromeric DNA sequence elements (Hornung et al., 2014), kinetochore assemblies that relied on OA were significantly stronger when assembled on CCEN-NCPs relative to those assembled on W601-NCPs ($p=1.87x10^{-6}$). The median rupture force for OA-based assemblies on CCEN-NCPs was 6.0 pN compared to the W601-NCP median of 4.2 pN (Figure 2B and 2C).

W601 Mif2 vs. CCEN Mif2

CCEN-NCP assemblies with Mif2 were not significantly stronger than assemblies with W601-NCPs (p=0.302), which was surprising given that the CDEII region of the centromere that contains a Mif2-binding footprint (Xiao et al., 2017) was present in our chimera. The median rupture force for Mif2-based assemblies on CCEN-NCPs was 2.9 pN, which was slightly higher but not significantly different than the W601-NCP median of 2.5 pN (Figure 2B and 2C).

Discussion

Previous work showed that OA nonspecifically binds to both CEN3 and non-CEN3 free DNA fragments, suggesting a sequence-independent OA-DNA binding interaction (Hornung et al., 2014). OA is also known to bind the unstructured N-terminus of Cse4 (Anedchenko et al., 2019; Fischbock-Halwachs et al., 2019; Shukla et al., 2024). Here we find that the strength of OA-based assemblies, when tested in the context of wrapped nucleosomes, is higher when the nucleosomes are wrapped with a CEN3-containing DNA sequence versus when the nucleosomes are wrapped with W601 DNA. This result together with that of Hornung and coworkers (Hornung et al., 2014) implies a difference in the importance of centromeric DNA sequences when OA binds to free DNAs as opposed to DNA wrapped around a nucleosome. We propose two possibilities to rationalize this difference. First, the effect could be indirect; an NCP wrapped with the chimeric CCEN DNA might present the N-terminal tail of Cse4 more favorably to OA, thereby increasing the rupture strength of OA-mediated kinetochore assemblies. Alternatively, OA could demonstrate sequence preferences but only when the DNA is bent around a nucleosome

and not when presented as free DNA. In support of this possibility, the recent structure of the inner kinetochore wrapped around a nucleosome shows that a small segment of OA is near the wrapped DNA (Dendooven et al., 2023).

Xiao and coworkers (Xiao et al., 2017) showed that both Cse4 and CEN DNA contribute to Mif2 binding to centromeric nucleosomes. Our prior work found that Mif2-based kinetochore assemblies could form on Cse4 containing nucleosomes wrapped with W601 DNA but not on H3-containing nucleosomes wrapped with W601 DNA (Hamilton et al., 2020), as expected given the 100-fold lower affinity Mif2 has for H3 based nucleosomes (Xiao et al., 2017). Xiao and coworkers (Xiao et al., 2017) also found that Mif2 has a 30-fold higher affinity for CEN3 DNA wrapped nucleosomes than for nucleosomes wrapped with pericentromeric DNA and 100-fold higher affinity compared to nucleosomes wrapped with W601 DNA. They showed that Mif2 footprints a thirty-five base pair section at the end of CDEII in CEN3. Here we wrapped Cse4 nucleosomes with CCEN DNA, which includes all thirty-five base pairs of the Mif2 footprint in CDEII and compared their properties to those wrapped with W601 DNA. In our experiments, Mif2 did not exhibit DNA sequence specificity for CCEN over W601. A key difference between CCEN and CEN3 DNA is that CCEN is missing 47 bp of CDEII. Our results suggest that the increased affinity of Mif2 for CEN3 DNA observed by Xiao and coworkers might require more than just the portion of CDEII that is footprinted by Mif2. Current structures of the yeast inner kinetochore assembled on NCPs either do not include Mif2 or reveal only a peptide of it (Dendooven et al., 2023; Yan et al., 2019) . Our results suggest that a substantial portion of CEN3 might be required to stably assemble Mif2 on the NCP.

It has not yet been possible to obtain structures of yeast NCPs wrapped in authentic CEN3 DNA without using some method to stabilize the NCPs. Guan and coworkers solved a structure of yeast centromeric CEN3 DNA-wrapped NCPs bound to a stabilizing antibody. This structure did not include inner kinetochore proteins (Guan et al., 2021). Three structures of yeast NCPs bound to inner kinetochore components have also been solved (Dendooven et al., 2023; Guan et al., 2021; Yan et al., 2019), all of which relied either on W601 DNA or hybrid DNAs that contained six bp of CDEII, all of CDEIII, and sequences downstream of CDEIII. Here we describe a new chimera of CEN3 and W601 DNA (CCEN) that includes 35 bp of CDEII as well as all of CDEIII and the region downstream of CDEIII. CCEN stably wrapped yeast centromeric histone octamers and revealed new DNA sequence preferences not previously appreciated.

Conclusion

We have developed a chimeric DNA sequence (CCEN) that represents an advance towards working with a more native-like recombinant kinetochore. Using centromeric nucleosomes wrapped with CCEN DNA, we have confirmed previous findings that OA and Mif2 can independently support recombinant kinetochore assembly. We showed previously that they can distinguish centromeric versus non-centromeric nucleosomes based on histone identity (Hamilton et al., 2020). Here we provide the first evidence that OA also distinguishes between centromeric and non-centromeric nucleosomes on the basis of DNA sequence. We also show that Mif2 requires more than the DNA binding site identified by footprinting to display sequence preferences.

Materials and Methods

Plasmids

Plasmids are listed in Table 2. Plasmid pAZ144 was derived from pSc_Mf_7, which expressed Mif2-linker-(27-392)MBP-6XHis (Hamilton et al., 2020). Agilent's QuikChange Lightning Site-Directed Mutagenesis Kit (product number: 210518) was used according to the manufacturer's instructions to loop out the 6XHis tag from pSc_Mf_7 and to modify the C terminal end of the MBP tag to make it identical to the E. coli MBP protein. To this end amino acids GSSHHHHHH were removed and replaced with the native C terminal sequence of the E. coli MBP protein (QTRITK) resulting in a new coding sequence encoding Mif2-linker-(27-392)MBP. The forward and reverse primers used for this were GAAAGACGCGCAGACTCGTATTACCAAATAATAAACCAACTCCATAAGG and CCTTATGGAGTTGGTTTATTATTTGGTAATACGAGTCTGCGCGTCTTTC, respectively. In all other respects pAZ144 was identical to pSc_Mf_7. Plasmids are available from the corresponding author.

Design of chimeric centromeric DNA sequence

The chimeric centromeric DNA sequence (CCEN) is a chimera of CEN3 and Widom 601 DNA. CCEN is 147 bp long and includes four elements: i) the first 62 bp of W601, ii) 35 bp of CDEII that includes the Mif2 footprint (Xiao et al., 2017), iii) the rest of the CBF 3 binding site (Guan et al., 2021), which is all of CDEIII (25 bp) and 17 bp downstream of CDEIII, and iv) the last 8 bp of W601. (Note that the 48-bp CBF3 binding site overlaps with the last 6 bp of the Mif2 binding site (Guan et al., 2021).) Of 5 CEN3-W601 chimeras tested, CCEN was the only one that included the Mif2 and CBF3 binding sites and stably wrapped centromeric histone octamers such that the nucleosomes could be further purified by size

exclusion chromatography. Specifically, a construct containing only CEN3 did not stably wrap histone octamers in our hands.

NCP wrapping

Yeast histones were purified as described (Hamilton et al., 2020). W601 DNA and CCEN DNA were purchased from Integrated DNA Technologies. Mononucleosome core particles were reconstituted by the standard salt dialysis method as described (Witus et al., 2023) with two exceptions. First, the nucleosomes contained *S. cerevisiae* histones Cse4, H2A, H2B, and H4, the latter three were tagged with 6X-His. Second, the W601 DNA and histones were combined in a 1:1.80 molar ratio, while CCEN DNA and histones were combined in a 1:1.55 molar ratio. Nucleosomes were further purified by size exclusion chromatography using a 24 ml Superdex 200 increase 10/300 column equilibrated in NCP storage buffer (30 mM HEPES buffer (pH 7.5), 10 mM NaCl, 0.1 mM EDTA, 0.5 mM TCEP). NCPs purified by size exclusion chromatography were stored on ice at 4˚C and used within 5 days of purification.

Purification of Kinetochore Proteins

OA, Mif2, MIND, Ndc80c, and Dam1c were expressed as described with slight modifications (Hamilton et al., 2020). Briefly, each complex was expressed from a polycistronic vector (Table 2) in Rosetta 2 DE3 pLysS cells (Novagen). Cells were grown to OD_{600} = 0.6 and induced with 0.3 mM isopropyl β-D-1-thiogalactopyranoside (IPTG) for 16-18 hours at 18˚C. After the induction period, cells were pelleted and washed with PBS containing 1 mM PMSF. Cell pellets were frozen in liquid nitrogen and stored at -80˚C until purification.

MIND-FLAG

On the day of purification, cell pellets were resuspended in MIND-lysis buffer (Table 3), and cells were lysed using a French Press and lysates were cleared by high-speed centrifugation. The cleared lysate was incubated with 2 ml of MonoRab anti-DYKDDDDK Affinity Resin (L0076; GenScript) for 30 minutes. After the resin was washed with 10 column volumes of MIND-wash buffer (Table 3), the immobilized protein was incubated for 30 min with MIND-elution buffer (Table 3) containing 200 µg/mL 3x FLAG peptide (F4799; Sigma). Eluate from the anti-FLAG resin was collected and further purified by size exclusion chromatography in MIND-SEC buffer on a 120 mL Superdex 200 column (28-9893-35; GE Healthcare). Eluted fractions were pooled and concentrated if necessary using an Amicon Ultra centrifugal filter (UFC805008; Millipore). Purified protein was stored in MIND-SEC buffer with 5% glycerol at -80˚C. Protein concentration was measured via the bicinchoninic acid assay (Thermo Fisher and Sigma Aldrich).

OA-FLAG

OA-FLAG was purified as described for MIND-FLAG except that the OA-lysis, OA-elution, and OA-SEC buffers listed in Table 3 were used. Additionally, the immobilized OA on the FLAG resin was washed with 8 column volumes of OA-High Salt-Wash and 2 column volumes of OA-Low Salt-Wash prior to elution in order to remove co-purifying bacterial DNA.

Mif2-MBP

Mif2-MBP was purified as described (Hamilton et al., 2020), with three exceptions. First, the Mif2-lysis, Mif2-amylose elution, Mif2-QA, and Mif2-QB, buffers that are listed in

Table 3 were used. Second, Mif2 was eluted from the anion exchange column with a 0-80% gradient of QB. Third, Mif2 was not subjected to size exclusion chromatography.

Ndc80c-FLAG

Ndc80c-FLAG was purified as described for MIND-FLAG with two exceptions. First the Ndc80c-lysis, Ndc80c-wash, Ndc80c-elution, and Ndc80c-SEC buffers listed in Table 3 were used. Second, the eluate from the FLAG affinity resin was concentrated in a 50 kDa molecular weight cutoff concentrator prior to loading on the Superdex 200 column.

Dam1c-FLAG

Dam1c-FLAG was purified as described for MIND-FLAG, except the Dam1c-lysis, Dam1c-wash, Dam1c-elution, and Dam1c-SEC specific buffers listed in Table 3 were used.

Optical Trap Assay

Slide preparation for the optical trap assay was performed as previously described (Flores et al., 2022; Hamilton et al., 2020) with changes to the buffers listed below. 40 nM His6-NCPs and anti-His6 beads were incubated in bead incubation buffer (30 mM HEPES (pH 7.5), 10 mM NaCl, 1 mM EDTA, 0.5 mM TCEP, 2 mg/mL κ-casein) for 30 min. All kinetochore proteins were diluted in a buffer containing 1x BRB80 (80 mM PIPES pH 6.9, 1 mM $MgCl_2$, 1 mM EGTA) and 2 mg/mL κ-casein before addition to the reaction mix. The reaction mix contained 1x BRB80, 1 mM GTP, 8 mg/mL BSA, 0.05 mg/mL biotinylated BSA, 0.8 mM DTT, 250 µg/mL glucose oxidase, 30 µg/mL catalase, 3.6 mg/mL glucose, and 16 µM tubulin in addition to the non-His6 tagged proteins free in solution. 10 nM OA or 20 nM Mif2, 10 nM 2D-MIND, 10 nM Ndc80c, and 5 nM Dam1c were used in the trapping assays. Optical

trap assays were performed at room temperature using custom instrumentation to capture and manipulate beads as described (Franck et al., 2010). Rupture force assays were performed as described (Hamilton et al., 2020). Once beads were bound to microtubule tips, a test force of 1 pN was applied, and only beads that tracked with ~100 nm of tip growth were subjected to ramping force of 0.25 pNs until detachment. All attachments that withstood the 1 pN preload force were included in our analysis. Each slide was used to collect data for no more than 90 minutes.

Data Analysis and Visualization

Igor Pro (Wavemetrics) was used to analyze data from optical trap assays and generate graphs for figures. Adobe Illustrator was used to generate figures.

Acknowledgements

We thank Mai Bayarjargal, Emmanuel Boakye-Ansah and Eric Muller for helpful discussions. This work was funded by NIH Grants R35GM130293 to TND, R35GM134842 to CLA, and R01CA260834 to REK. The authors declare no competing financial interests.

Figure legends

Figure 1. Recombinantly wrapped NCPs with W601 or CCEN DNA.

A) Sequences of the W601 and CCEN DNA used to wrap histone octamers. The black text is W601 DNA, the blue text is the Mif2 footprint within CDEII (Xiao et al., 2017), the green text is CDEIII, the sequence underlined in green is the CBF3 binding site (Guan et al., 2021) and the red text is the pericentromeric DNA sequence just downstream of CDEIII on chromosome III. B) Chromatogram representing elution fractions from size exclusion

chromatography column used to purify wrapped NCPs from excess free DNA. 260 nm signal is shown for both W601 and CCEN NCPs. C) Native gel of elution fractions indicated in the chromatogram in B. NCPs from both SEC Fraction 6 and SEC Fraction 7 were used to collect data on the optical trap. There was no statistically significant difference between rupture forces of assemblies measured with NCPs from either Fraction 6 or Fraction 7.

Figure 2. Kinetochore assemblies built on CCEN-NCPs and OA form stronger attachments to microtubules.

A) Percentages of beads that had microtubule binding capability. Error bars indicate the standard error of the proportion. Barnard's test was used to compare contingency tables. The p-values for the significance of the difference between fraction of beads bound if either OA or Mif2 were included compared to if neither were included are given in Table 1. Data were combined from two biological replicates (See Source Data table). B) Boxplot of rupture forces for each of the kinetochore assemblies tested. Dots represent individual rupture events, and boxes enclose the interquartile range, with indicated medians. Whiskers extend to the inner fences. Data were combined from four biological replicates of each condition (see Source Data Table). A Kolmogorov-Smirnov test was performed to compare the probability distributions of rupture forces across conditions. *** indicates p-value of 1.87×10^{-6}, n.s., not significant. C) Survival probability curves for the data plotted in B.

Tables

Table 1: Statistical analyses for microtubule binding assay[1]

Condition	CCEN NCP neither OA nor Mif2	W601 NCP neither OA nor Mif2
W601 NCP, OA	N/A[2]	2.61×10^{-12}
CCEN NCP, OA	3.55×10^{-13}	N/A
W601 NCP, Mif2	N/A	2.31×10^{-12}
CCEN NCP, Mif2	4.27×10^{-7}	N/A

[1]p-values for comparison of data in Figure 2A determined by a Barnard's test
[2]Not applicable

Table 2: Plasmids used for expression of kinetochore proteins[1]

Protein	Plasmid	Components	References
Nucleosome	pScKl2	*K. lactis* 6XHis-H2A, *K. lactis* 6XHis-H2B, Cse4, *K. lactis* 6XHis-H4	(Migl et al., 2020)
OA	pGH3	Okp1, Ame1-FLAG	(Hamilton et al., 2020)
Mif2	pAZ144	Mif2-MBP	This study
2D-MIND	pGH62	FLAG-Nsl1, S240D & S250D Dsn1, Mtw1, Nnf1	(Hamilton et al., 2020)

(230-576) 2D-MIND	pEHM4	FLAG-Nsl1, (230-576) S240D & S250D Dsn1, Mtw1, Nnf1	(Hamilton et al., 2020)
Ndc80c	pJT48 Ndc80/Nuf2	Spc24-FLAG, Spc25 Ndc80, Nuf2	(Kudalkar et al., 2015) (Wei et al., 2005)
Dam1c	pJT44	Spc34-FLAG, Dad1, Dad2, Dad3, Dad4 Duo1, Dam1, Hsk3, Spc19, Ask1	(Umbreit et al., 2014)

[1]All proteins are from *Saccharomyces cerevisiae* except as noted.

Table 3: Kinetochore protein purification buffers.

Protein	Purification Buffers
Dam1c-FLAG	**Lysis:** 50 mM sodium phosphate buffer pH 6.9, 500 mM NaCl, 1 mM PMSF, Roche protease inhibitor tablets **FLAG Wash:** 50 mM sodium phosphate buffer pH 6.9, 500 mM NaCl, 1 mM PMSF, Roche protease inhibitor tablets **FLAG Elution:** 50 mM sodium phosphate buffer pH 6.9, 500 mM NaCl, 1 mM PMSF, Roche protease inhibitor tablets, 200 ug/mL 3x FLAG peptide **SEC:** 50 mM sodium phosphate buffer pH 6.9, 500 mM NaCl
Mif2-MBP	**Lysis:** 30 mM HEPES buffer pH 7.5, 2M NaCl, 10% glycerol, 1 mM TCEP, 1 mM PMSF, Roche protease inhibitor tablets **Amylose Resin Elution:** 30 mM HEPES buffer pH 7.5, 100 mM NaCl, 10% glycerol, 1 mM TCEP, 1 mM PMSF, Roche protease inhibitor tablets, 10 mM maltose **QA:**

	30 mM HEPES buffer pH 7.5, 100 mM NaCl, 10% glycerol, 1 mM TCEP, 1 mM PMSF, Roche protease inhibitor tablets **QB**: 30 mM HEPES buffer pH 7.5, 1M NaCl, 10% glycerol, 1 mM TCEP
MIND-FLAG	**Lysis:** 50 mM HEPES buffer pH 7.5, 200 mM NaCl, 10% glycerol, 0.5% NP40, 1 mM EDTA, 1 mM PMSF, Roche protease inhibitor tablets **FLAG Wash:** 50 mM HEPES buffer pH 7.5, 200 mM NaCl, 10% glycerol, 1 mM EDTA, 1 mM PMSF, Roche protease inhibitor tablets **FLAG Elution:** 50 mM HEPES buffer pH 7.5, 200 mM NaCl, 10% glycerol, 1 mM EDTA, 1 mM PMSF, Roche protease inhibitor tablets, 200 ug/mL 3x FLAG peptide **SEC:** 50 mM HEPES buffer pH 7.5, 200 mM NaCl, 1 mM EDTA
Ndc80c-FLAG	**Lysis:** 50 mM HEPES buffer pH 7.6, 200 mM NaCl, 10% glycerol, 1 mM EDTA, 1 mM PMSF, Roche protease inhibitor tablets **FLAG Wash:** 50 mM HEPES buffer pH 7.6, 200 mM NaCl, 10% glycerol, 1 mM EDTA, 1 mM PMSF, Roche protease inhibitor tablets **FLAG Elution:**

	50 mM HEPES buffer pH 7.6, 200 mM NaCl, 10% glycerol, 1 mM EDTA, 1 mM PMSF, Roche protease inhibitor tablets, 200 ug/mL 3x peptide **SEC:** 50 mM HEPES buffer pH 7.6, 200 mM NaCl, 1 mM EDTA
OA-FLAG	**Lysis:** 50 mM HEPES buffer pH 7.5, 200 mM NaCl, 10% glycerol, 0.5% NP40, 1 mM PMSF, Roche protease inhibitor tablets **Low Salt FLAG Wash:** 50 mM HEPES buffer pH 7.5, 200 mM NaCl, 10% glycerol, 1 mM EDTA, 1 mM PMSF, Roche protease inhibitor tablets **High Salt FLAG Wash:** 50 mM HEPES buffer pH 7.5, 2 M NaCl, 10% glycerol, 1 mM EDTA, 1 mM PMSF, Roche protease inhibitor tablets **FLAG elution:** 50 mM HEPES buffer pH 7.5, 200 mM NaCl, 10% glycerol, 1 mM EDTA, 1 mM PMSF, Roche protease inhibitor tablets, 200 ug/mL 3x FLAG peptide **SEC:** 50 mM HEPES buffer pH 7.5, 200 mM NaCl, 1 mM EDTA

References

Akiyoshi, B., K.K. Sarangapani, A.F. Powers, C.R. Nelson, S.L. Reichow, H. Arellano-Santoyo, T. Gonen, J.A. Ranish, C.L. Asbury, and S. Biggins. 2010. Tension directly stabilizes reconstituted kinetochore-microtubule attachments. *Nature*. 468:576-579.

Anedchenko, E.A., A. Samel-Pommerencke, T.M. Tran Nguyen, S. Shahnejat-Bushehri, J. Popsel, D. Lauster, A. Herrmann, J. Rappsilber, A. Cuomo, T. Bonaldi, and A.E. Ehrenhofer-Murray. 2019. The kinetochore module Okp1(CENP-Q)/Ame1(CENP-U) is a reader for N-terminal modifications on the centromeric histone Cse4(CENP-A). *EMBO J*. 38.

Ariyoshi, M., and T. Fukagawa. 2023. An updated view of the kinetochore architecture. *Trends Genet*. 39:941-953.

Clarke, L., and J. Carbon. 1980. Isolation of a yeast centromere and construction of functional small circular chromosomes. *Nature*. 287:504-509.

Clarke, L., and J. Carbon. 1985. The structure and function of yeast centromeres. *Annu Rev Genet*. 19:29-55.

Dendooven, T., Z. Zhang, J. Yang, S.H. McLaughlin, J. Schwab, S.H.W. Scheres, S. Yatskevich, and D. Barford. 2023. Cryo-EM structure of the complete inner kinetochore of the budding yeast point centromere. *Sci Adv*. 9:eadg7480.

Fischbock-Halwachs, J., S. Singh, M. Potocnjak, G. Hagemann, V. Solis-Mezarino, S. Woike, M. Ghodgaonkar-Steger, F. Weissmann, L.D. Gallego, J. Rojas, J. Andreani, A. Kohler, and F. Herzog. 2019. The COMA complex interacts with Cse4 and positions Sli15/Ipl1 at the budding yeast inner kinetochore. *Elife*. 8.

Flores, R.L., Z.E. Peterson, A. Zelter, M. Riffle, C.L. Asbury, and T.N. Davis. 2022. Three interacting regions of the Ndc80 and Dam1 complexes support microtubule tip-coupling under load. *J Cell Biol*. 221.

Franck, A.D., A.F. Powers, D.R. Gestaut, T.N. Davis, and C.L. Asbury. 2010. Direct physical study of kinetochore-microtubule interactions by reconstitution and interrogation with an optical force clamp. *Methods*. 51:242-250.

Guan, R., T. Lian, B.R. Zhou, E. He, C. Wu, M. Singleton, and Y. Bai. 2021. Structural and dynamic mechanisms of CBF3-guided centromeric nucleosome formation. *Nat Commun*. 12:1763.

Hamilton, G.E., L.A. Helgeson, C.L. Noland, C.L. Asbury, Y.N. Dimitrova, and T.N. Davis. 2020. Reconstitution reveals two paths of force transmission through the kinetochore. *eLife*. 9:e56582.

Hornung, P., P. Troc, F. Malvezzi, M. Maier, Z. Demianova, T. Zimniak, G. Litos, F. Lampert, A. Schleiffer, M. Brunner, K. Mechtler, F. Herzog, T.C. Marlovits, and S. Westermann. 2014. A cooperative mechanism drives budding yeast kinetochore assembly downstream of CENP-A. *J Cell Biol*. 206:509-524.

Kudalkar, E.M., E.A. Scarborough, N.T. Umbreit, A. Zelter, D.R. Gestaut, M. Riffle, R.S. Johnson, M.J. MacCoss, C.L. Asbury, and T.N. Davis. 2015. Regulation of outer kinetochore Ndc80 complex-based microtubule attachments by the central

kinetochore Mis12/MIND complex. *Proceedings of the National Academy of Sciences of the United States of America*. 112:E5583-E5589.

Lowary, P.T., and J. Widom. 1998. New DNA sequence rules for high affinity binding to histone octamer and sequence-directed nucleosome positioning. *J Mol Biol*. 276:19-42.

Migl, D., M. Kschonsak, C.P. Arthur, Y. Khin, S.C. Harrison, C. Ciferri, and Y.N. Dimitrova. 2020. Cryoelectron Microscopy Structure of a Yeast Centromeric Nucleosome at 2.7 A Resolution. *Structure*. 28:363-370 e363.

Nicklas, R.B., and S.C. Ward. 1994. Elements of error correction in mitosis: microtubule capture, release, and tension. *J Cell Biol*. 126:1241-1253.

Shukla, S., A. Bhattacharya, P. Sehrawat, P. Agarwal, R. Shobhawat, N. Malik, K. Duraisamy, N.S. Rangan, R.V. Hosur, and A. Kumar. 2024. Disorder in CENP-A(Cse4) tail-chaperone interaction facilitates binding with Ame1/Okp1 at the kinetochore. *Structure*. 32:690-705 e696.

Umbreit, N.T., M.P. Miller, J.F. Tien, J.C. Ortolá, L. Gui, K.K. Lee, S. Biggins, C.L. Asbury, and T.N. Davis. 2014. Kinetochores require oligomerization of Dam1 complex to maintain microtubule attachments against tension and promote biorientation. *Nat Commun*. 5:4951.

Wei, R.R., P.K. Sorger, and S.C. Harrison. 2005. Molecular organization of the Ndc80 complex, an essential kinetochore component. *Proc Natl Acad Sci U S A*. 102:5363-5367.

Witus, S.R., L.M. Tuttle, W. Li, A. Zelter, M. Wang, K.E. Kermoade, D.B. Wilburn, T.N. Davis, P.S. Brzovic, W. Zhao, and R.E. Klevit. 2023. BRCA1/BARD1 intrinsically disordered regions facilitate chromatin recruitment and ubiquitylation. *EMBO J*. 42:e113565.

Xiao, H., F. Wang, J. Wisniewski, A.K. Shaytan, R. Ghirlando, P.C. FitzGerald, Y. Huang, D. Wei, S. Li, D. Landsman, A.R. Panchenko, and C. Wu. 2017. Molecular basis of CENP-C association with the CENP-A nucleosome at yeast centromeres. *Genes Dev*. 31:1958-1972.

Yan, K., J. Yang, Z. Zhang, S.H. McLaughlin, L. Chang, D. Fasci, A.E. Ehrenhofer-Murray, A.J.R. Heck, and D. Barford. 2019. Structure of the inner kinetochore CCAN complex assembled onto a centromeric nucleosome. *Nature*. 574:278-282.

A

W601 sequence:
ATCGAGAATCCCGGTGCCGAGGCCGCTCAATTGGTCGTAGACAGCTCTAGCACCGCTTAAAC
GCACGTACGCGCTGTCCCCCGCGTTTTAACCGCCAAGGGGATTACTCCCTAGTCTCCA GGCACGTGTCAGATATATA
CATCCGAT

CCEN sequence:
ATCGAGAATCCCGGTGCCGAGGCCGCTCAATTGGTCGTAGACAGCTCTAGCACCGCTTAAAC
AGTTTATTTTTAAAAAATAAAATTTAAAATATTAGTGTATTTGATTTCCGAAAGTTAAAAAAGAAATAGTAAGAAAT
CATCCGAT

Key:
W601 DNA, CDEII, CDEIII,
downstream of CDEIII

B

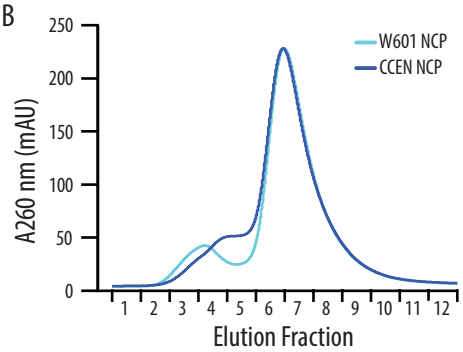

C

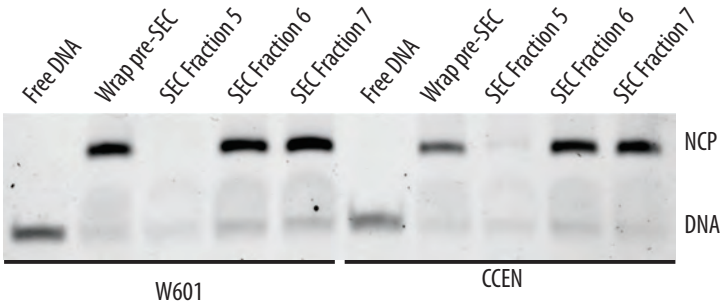

Figure 1. Recombinantly wrapped NCPs with W601 or CCEN DNA. A) Sequences of the W601 and CCEN DNA used to wrap histone octamers. The black text is W601 DNA, the blue text is the Mif2 footprint within CDEII (Xiao et al., 2017), the green text is CDEIII, the sequence underlined in green is the CBF3 binding site (Guan et al., 2021) and the red text is the pericentromeric DNA sequence just downstream of CDEIII on chromosome III. B) Chromatogram representing elution fractions from size exclusion chromatography column used to purify wrapped NCPs from excess free DNA. 260 nm signal is shown for both W601 and CCEN NCPs. C) Native gel of elution fractions indicated in the chromatogram in B. NCPs from both SEC Fraction 6 and SEC Fraction 7 were used to collect data on the optical trap. There was no statistically significant difference between rupture forces of assemblies measured with NCPs from either Fraction 6 or Fraction 7.

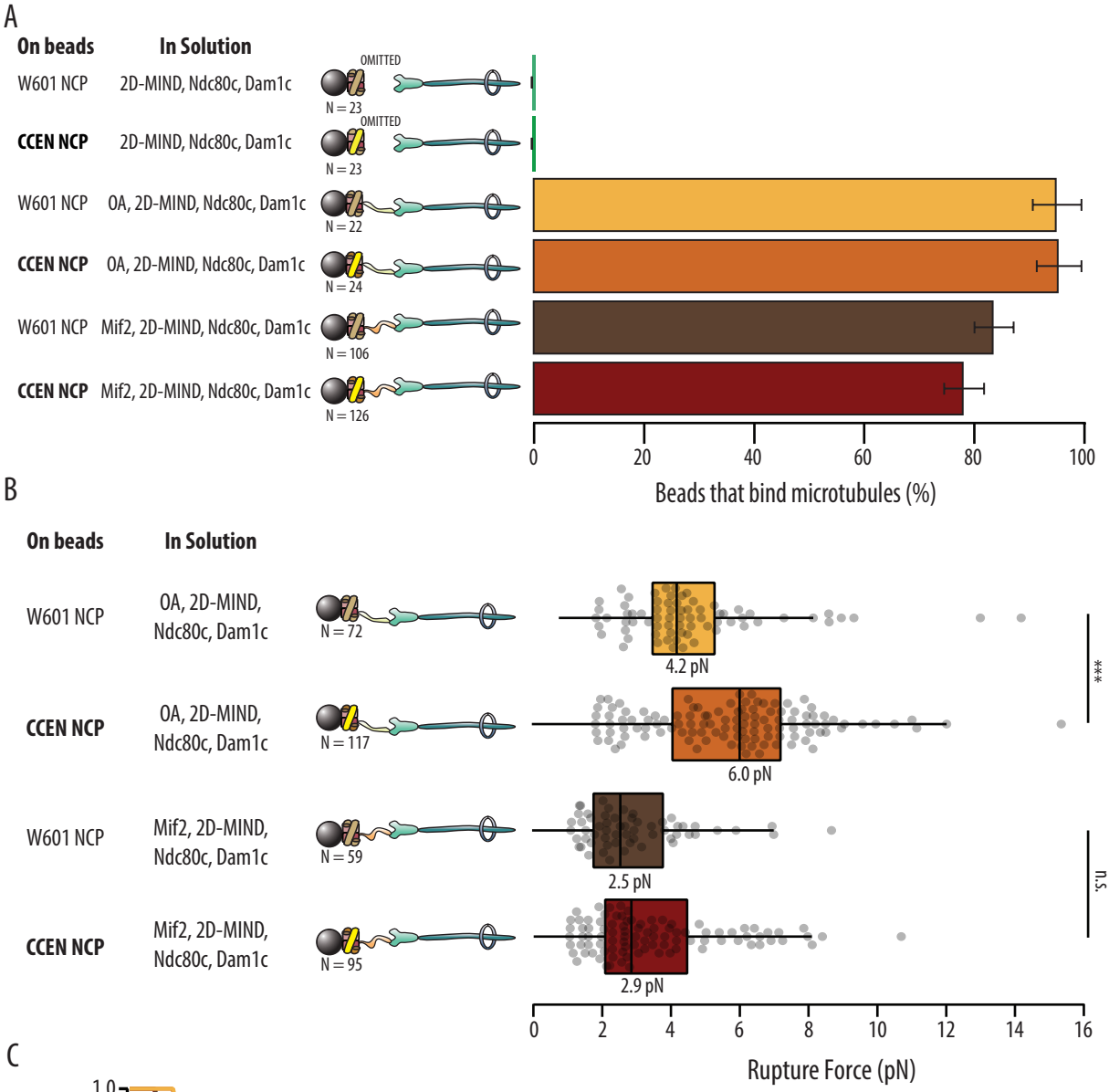

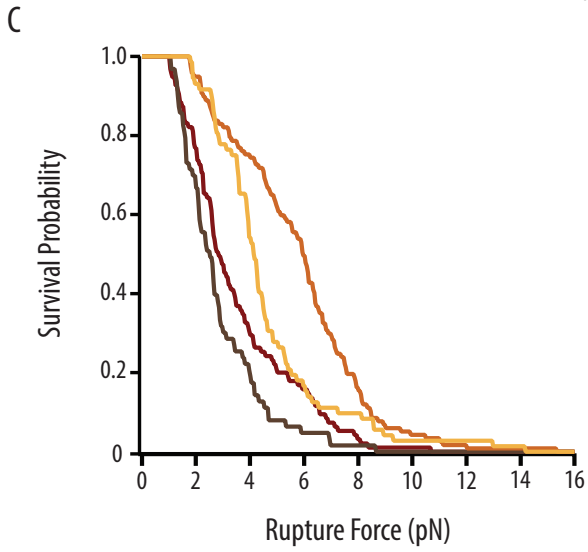

Figure 2. Kinetochore assemblies built on CCEN-NCPs and OA form stronger attachments to microtubules.
A) Percentages of beads that had microtubule binding capability. Error bars indicate the standard error of the proportion. Barnard's test was used to compare contingency tables. The p-values for the significance of the difference between fraction of beads bound if either OA or Mif2 were included compared to if neither were included are given in Table 1. Data were combined from two biological replicates (See Source Data table). B) Boxplot of rupture forces for each of the kinetochore assemblies tested. Dots represent individual rupture events, and boxes enclose the interquartile range, with indicated medians. Whiskers extend to the inner fences. Data were combined from four biological replicates of each condition (see Source Data Table). A Kolmogorov-Smirnov test was performed to compare the probability distributions of rupture forces across conditions. *** indicates p-value of 1.87 x 10-6, n.s., not significant. C) Survival probability curves for the data plotted in B.